

Strength of Faults on Mars from MOLA Topography

David N. Barnett and Francis Nimmo

Bullard Laboratories of the Department of Earth Sciences, University of Cambridge, Madingley Road, Cambridge CB3 0EZ, United Kingdom
E-mail: barnett@esc.cam.ac.uk

Received August 21, 2001; revised November 12, 2001

The stresses which must be maintained on faults bounding the rift topography at Tempe Fossae—the “North Tempe Rift” (NTR)—and Valles Marineris (VM) on Mars are estimated, using a simple elastic model and topographic data from the Mars Orbiter Laser Altimeter (MOLA). The absence of rift-flank uplift at the NTR is consistent with an elastic thickness, T_e , of 20 km or greater at the time of rift formation. The maximum resolved shear stresses on bounding faults due to this topography do not therefore exceed 20 MPa, similar to the inferred strength of terrestrial faults. Elastic thickness estimates at VM are mostly around 50 km or greater. Therefore, for canyon widths of ~ 400 km, the bounding faults of VM, if present, must be able to withstand stresses of up to approximately 100 MPa. However, if the fault-controlled sections of the canyons do not exceed 150 km in width, as suggested by geomorphological analysis, the fault strength required is only 20 MPa. Although the maximum resolved shear stresses required to support the topography at VM may need to be greater than the stresses which terrestrial faults can support, at least some faults on Mars are no stronger than similar features on Earth. This observation is consistent with the existence of liquid water in the shallow subsurface of Mars at the time the faults were active. On Venus, plate tectonics is probably prevented by the frictional resistance to motion across strong faults. On Mars, it is more likely that the large thickness of the elastic layer of the lithosphere and the possible positive buoyancy of the crust are responsible for the observed lack of plate tectonics. © 2002 Elsevier Science (USA)

Key Words: Mars; faults; stress; rifts; elastic thickness; plate tectonics.

1. INTRODUCTION

On Earth it has been observed that the strain, \bar{u}/L , associated with active faulting in earthquakes is always approximately 10^{-5} , regardless of the dimensions of the fault, where \bar{u} is the average displacement on the fault during one earthquake and L is its length (Scholz 1982). The corresponding stress drop, $\Delta\sigma$, is related to the strain by

$$\Delta\sigma = \mu \frac{\bar{u}}{L}, \quad (1)$$

where μ is the rigidity modulus of the rock. The stress drops observed in large earthquakes are therefore between 1 and 10 MPa.

This value is far smaller than the frictional stress of several hundred MPa which one would predict should exist on fault planes at earthquake depths, on the basis of the magnitude of lithostatic pressure and the fact that the coefficient of friction is approximately constant (around 0.6) over a wide depth range (Byerlee 1968, Barton 1976, Byerlee 1978, Brace and Kohlstedt 1980). Measurements of the heat flow anomalies across the San Andreas fault, where heat is being produced as a result of the work done against friction during fault movement, suggest that the maximum fault shear stress cannot be higher than around 20 MPa (Lachenbruch and Sass 1988), although this argument neglects heat lost by processes other than conduction (Scholz 2000). In addition, various authors (e.g., Mount and Suppe 1987, Zoback and Beroza 1993) have suggested, on the basis of fold axis orientations, aftershock mechanisms, and strain measurements in boreholes, that the maximum principal stress is roughly normal to that of the San Andreas and that the stress on the fault plane itself is small. However, palaeomagnetic measurements show that the folds have rotated by $25\text{--}30^\circ$ since they formed and may thus not reflect regional stress patterns (Scholz 2000). Finally, the observed occurrence of triggered left-lateral motion on small faults parallel to large right-lateral fault systems [the Hector Mine and North Anatolian faults (Wright *et al.* 2001)] also suggests that the stresses stored interseismically on these faults are small. In summary, therefore, the evidence suggests that the stress release in large earthquakes is of the same order as the total stress which may be stored on the fault, i.e., the fault *strength*. One explanation of the discrepancy between this value and that predicted by Byerlee’s law is that the presence of pore fluid could decrease the effective normal stress on the fault (i.e., weaken the fault) sufficiently, provided the pore fluid pressure was higher than the hydrostatic pressure at the time of rupture (Rice 1992). High pressures could be achieved by the effects of compaction or by the addition of water from metamorphic reactions within an impermeable seal of fault gouge. In this way, the pore fluid pressure might increase during an earthquake cycle, prior to rupture (Sleep and Blanpied 1992).

The strength of faults supporting rift valley topography may also be estimated from the geometry of the topography if the elastic thickness of the lithosphere is known. The elastic thickness, T_e , is the effective thickness of that part of the lithosphere

which can support elastic stresses over geological time scales. The thermal structure of the lithosphere is probably the primary control on T_e , with the base of the elastic layer occurring at the depth where the homologous temperature (the ratio of the absolute temperature to the melting temperature) is of order 0.6 (e.g., Watts 1994). The presence of small amounts of water reduces the melting temperature significantly and thus is likely to have an important weakening effect (e.g., in the continental mantle; Maggi *et al.* 2000). T_e is generally estimated using the correlation between gravity and topography in the frequency domain (e.g., Forsyth 1985, McKenzie and Fairhead 1997) or by modeling of flexural profiles in the space domain (e.g., Lyon-Caen and Molnar 1983, Nyquist and Wang 1988, McKenzie and Fairhead 1997).

Foster and Nimmo (1996) presented a comparative study of the strengths of the faults supporting the topography of two similarly sized rift valleys: the East African rift valley on Earth and Devana Chasma on Venus. They calculated the stress required to support the topography as a function of wavenumber, after the method of McKenzie (1967). Foster and Nimmo (1996) then showed that the analytical expressions of Jackson and White (1989), which approximate the fault block topography to a cosine curve, predict maximum resolved shear stresses, σ_{\max} , which are in good agreement with the numerical modeling. In the study by Jackson and White (1989), the value of σ_{\max} is given by

$$\sigma_{\max} = \frac{\rho_c g h}{2e} \quad \text{if } \frac{\lambda}{T_e} < \frac{\pi}{2} \quad (2a)$$

$$\sigma_{\max} = \frac{3\rho_c g h \lambda}{8\pi T_e} \quad \text{if } \frac{\pi}{2} < \frac{\lambda}{T_e} < \pi \quad (2b)$$

$$\sigma_{\max} = \frac{3\rho_c g h \lambda^2}{8\pi^2 T_e^2} \quad \text{if } \frac{\lambda}{T_e} > \pi, \quad (2c)$$

where ρ_c is the density of the faulted basement material, g is the acceleration due to gravity, $2h$ is the maximum vertical displacement associated with the faulting, e is the base of natural logarithms, and λ is the wavelength of the faulting. Devana Chasma exhibits fault lengths and vertical offsets similar to those of the East African rift valley but has wider half-grabens (about 150 km across). Since the elastic thickness is similar to that measured on the Earth (around 30 km) and there is an absence of sedimentary fill in the grabens in Venus, the faults on Venus must be able to withstand stresses of around 80 MPa, compared with around 10 MPa for East Africa. The stresses required to support the topography of the East African rift are therefore similar to the maximum stress drops observed in earthquakes. Thus, the amplitude of the topography is likely to be controlled by the strength of the supporting faults. The difference in fault strength between the two planets is probably due to the fact that the lithosphere on Venus is likely to be dry (McKenzie 1977, Nimmo and McKenzie 1998), so the faults are not weakened by pore fluid pressure as they are on Earth.

The existence of high-resolution topographic data for Mars now makes it possible to carry out similar studies for martian fault systems. The altimetry has been collected by the Mars Orbiter Laser Altimeter (MOLA) on the Mars Global Surveyor (MGS) spacecraft, from which several topographic grids, available on the MOLA Science Investigation Web site (<http://ftpwww.gsfc.nasa.gov/tharsis/mola.html>), have been derived. In this work, the $\frac{1}{16}^\circ$ resolution topographic model, IEG0062T, was used (Smith *et al.* 1999a), corresponding to a spatial resolution of about 4 km at the equator. The topographic value at each grid point in IEG0062T is equal to the difference between the planetary radius and the areoid at the same point. The accuracy of the MOLA topographic grids is vastly greater than that of previous digital terrain models, which typically had vertical errors of 1–3 km. The vertical uncertainty of the altimetry points in the 1° resolution model, for instance, is ± 13 m (Smith *et al.* 1999b).

2. THE NORTH TEMPE RIFT

2.1. Introduction

Tempe Fossae on Mars (the “North Tempe Rift” (NTR)) (approximately 44°N , 291°E – 50°N , 300°E) is similar in scale and geometry to terrestrial rift systems, and may have been formed in response to uplift due to an underlying mantle plume (Wilkins and Schultz 2001, Hauber and Kronberg 2001). The total length of the rift is around 500 km, but it is divided into a number of *en échelon* fault segments. In profile, the faults define a relatively symmetric full-graben structure, with a total width of around 100 km in the extreme north and south of the rift, and decreasing to around 50 km in the center, where the rift reaches its maximum depth of around 3 km (see Fig. 1). Assuming that the NTR is fault-bounded, the stresses which these faults must be capable of withstanding may be estimated using Eqs. (2a)–(2c). The topography at the NTR is not characteristic of the half-graben rifting for which these expressions were shown to be valid approximations, but the analytical expressions should give a rough estimate of the bounding fault strengths required for support of the topography.

2.2. Estimation of the Elastic Thickness at the North Tempe Rift

In order to estimate the value of σ_{\max} associated with the topography of a rift system, a reliable estimate of the elastic thickness, T_e , at that location is crucial. It is important to note that elastic thickness estimates produced by admittance analysis and flexural modeling will reflect the lowest strength of the lithosphere since the time at which the topographic loads were emplaced. Mars has been cooling with time, and therefore the lithospheric strength is likely to have been increasing. However, even if T_e has increased since the time of rift formation, the stresses in the original part of the elastic layer will remain unchanged. Therefore, it is the elastic thickness at the time of feature formation, as will be given by modeling the gravity or topography, which is required for calculation of σ_{\max} . Note

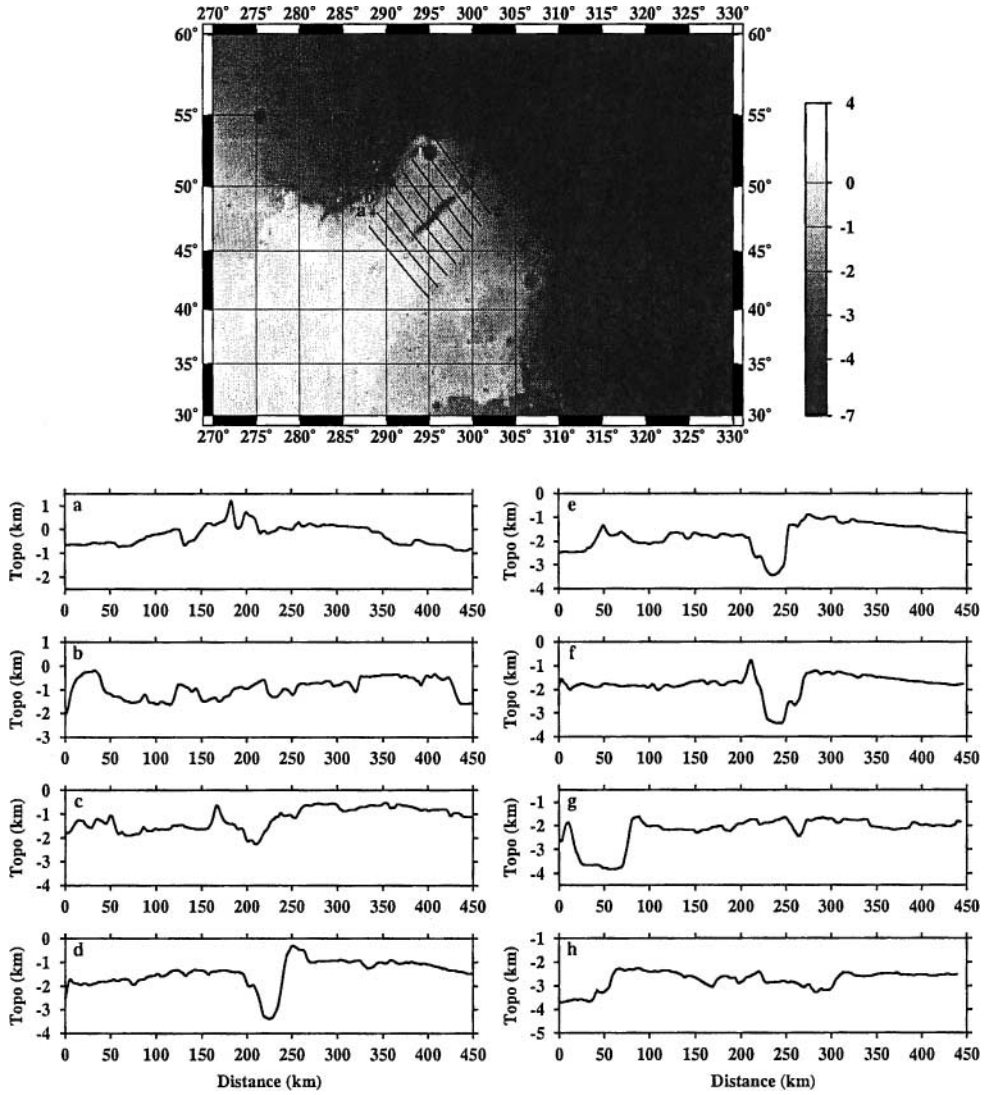


FIG. 1. Topographic profiles across the North Tempe Rift (NTR), taken from the $\frac{1}{16}^\circ$ resolution topographic model, IEG0062T (Smith *et al.* 1999a). The vertical exaggeration is about $\times 26$. The locations of the profiles are shown in the map at the top, showing planetary radius in km at each point, referenced to the areoid. Note that 10° latitude is approximately 600 km.

that the extension across Tempe Terra is thought to have occurred in two main phases (Golombek *et al.* 1996). The first, which produced more extension near Tharsis, occurred between the middle Noachian and early Hesperian (i.e., ~ 4 –3 Ga ago), while the subsequent phase of extension occurred between the late Hesperian and early Amazonian (i.e., ~ 3 –1 Ga ago) and produced more extension further from the Tharsis center (i.e., in the vicinity of the NTR). The absolute times are as given by Tanaka *et al.* (1992).

Since the elastic thickness at the NTR has not been measured, it was estimated in this work by considering the flexural uplift which would result from the emplacement of the rift, as a function of T_e . Figure 2 shows the topography which results when a 3-km-deep cosinusoidal trough, with width 50 km (i.e., similar to the dimensions of the NTR), is emplaced on a elastic plate

of varying thickness. The deflection of the plate was calculated using the method of McKenzie and Bowin (1976), which assumes a Cartesian geometry, using a thin plate approximation (Le Pichon *et al.* 1976). The plate deflection, $X(k)$, produced by a load, $S(k)$, is given by

$$X(k) = \frac{-S(k)\rho_c}{(1 + C_1 k'^4)\rho_m}, \quad (3)$$

in which

$$C_1 = \frac{2EM_\mu}{3\mu(1 - \sigma^2)} \quad (4)$$

$$k' = \left(\frac{T_e}{2}\right)k \quad (5)$$

and

$$M_\mu = \mu \left/ \left[g \rho_m \left(\frac{T_e}{2} \right) \right] \right. \quad (6)$$

This method assumes that the plate is incompressible. Hence, $\sigma = 0.5$ and $\mu = E/3$ (4.81×10^{10} Pa). All other parameter values are as given in Table I. The lack of any significant short-wavelength flexural uplift in the topographic profiles across the

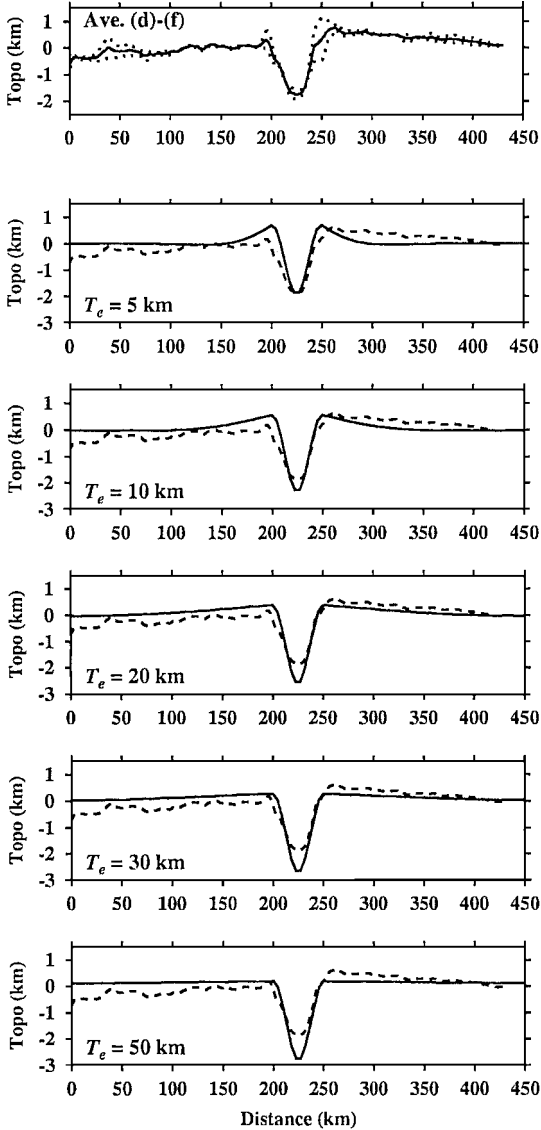


FIG. 2. The lowermost five plots show the resulting topography when a 3-km-deep cosinusoidal trough, with width 50 km (i.e., similar to the dimensions of the NTR), is emplaced on a plate of varying elastic thickness, T_e . The plate deflection was calculated according to the method of McKenzie and Bowin (1976), using a thin-plate approximation (Le Pichon *et al.* 1976). These may be compared with the top plot, which shows the average of topographic profiles (d), (e), and (f) across the NTR (as in Fig. 1; solid line) and also the topography plus and minus its standard deviation at each point (dotted lines). The average profile is also shown as a dashed line in the other plots.

TABLE 1
Parameter Values for Mars Used in This Study

g	Acceleration due to gravity	3.73 m s^{-2}
ρ_c	Crustal density	3.32 Mg m^{-3}
ρ_m	Density of the upper mantle	3.50 Mg m^{-3}
E	Young's modulus	$1.443 \times 10^{11} \text{ Pa}$
σ	Poisson's ratio	0.268

NTR (Figs. 1 and 2) is consistent with a T_e of greater than around 20 km. Note that this approach uses the very simple model of a continuous elastic plate with a (negative) top load; such an approach may be too simplistic in situations where rift-flanking faults are being modeled (Brown and Phillips 1999). In addition, the possibility of erosion of an original rift-flank uplift has been neglected; present-day erosion rates (Golombek and Bridges 2000) are too small to have any effect, although these rates were probably higher in the past.

2.3. Strength of Faults at the North Tempe Rift

Figure 3 shows the values of σ_{\max} calculated from Eqs. (2a)–(2c) as a function of λ and T_e , for two different values of h ; case (a) ($2h = 3$ km) is roughly appropriate for the NTR, while (b) ($2h = 8$ km) corresponds to Valles Marineris (Section 3). Note that σ_{\max} scales linearly with h . The densities and other material constants given in Table I are derived from the modal mineralogy of SNC meteorites, thought to be of martian origin (McKenzie and McSween, in preparation). The value of ρ_c is probably an upper limit, especially if water is present in the surficial layers of the crust, so that the obtained values of σ_{\max} are likely to be conservatively high.

For the NTR, the rift width (taken to be equal to the characteristic wavelength of faulting, λ) does not exceed 100 km (see Fig. 1). Figure 3a shows that, provided T_e at the NTR exceeds around 20 km, as is suggested by the flexural modeling in Section 2.2 (see Fig. 2), the faults at this location do not therefore need to support stresses greater than 20 MPa. Furthermore, the fact that the widest parts of the NTR tend to be somewhat shallower than 3 km (i.e., there is some suggestion of a trade-off between h and λ) also means that this upper limit on σ_{\max} is likely to be conservatively high.

3. VALLES MARINERIS

3.1. Introduction

Valles Marineris (VM) (approximately 5°S , 265°E – 15°S , 310°E) is a vast canyon system which is 4000 km long and up to 600 km wide where the individual canyons coalesce, reaching depths of 8–10 km in places (Lucchitta *et al.* 1992; see Fig. 4). The origin of the VM system is controversial, although it is likely that several processes contributed to its present structure. Tectonic processes, i.e., normal faulting and crustal rifting, produced in response to stresses related to the emplacement of

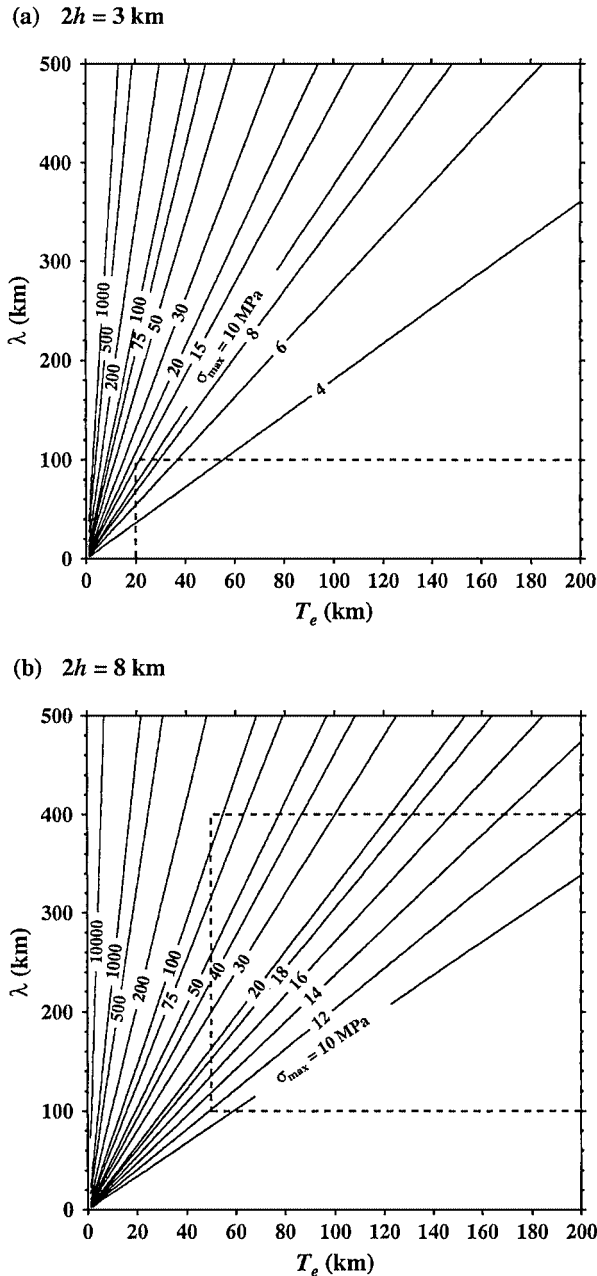


FIG. 3. Plots of the maximum shear stress, σ_{\max} , (in MPa), given by Eqs. 2a–2c, which assume a cosinusoidal form for the topography, as a function of wavelength, λ and elastic thickness, T_e , for the cases (a) in which $2h = 3$ km (i.e. appropriate for the NTR) and (b) $2h = 8$ km (i.e. appropriate for VM). The areas enclosed by dashed lines represent the regions of parameter space which are likely to be appropriate for the features in question; the ranges of λ are as given in Sections 2.1 and 3.2 and the ranges of T_e reflect the values discussed in Sections 2.2 and 3.1.

the large Tharsis volcanic center (Blasius *et al.* 1977, Banerdt *et al.* 1982, Sharp 1973, Frey 1979, Tanaka and Golombek 1989, review by Lucchitta *et al.* 1992), were probably responsible for the formation of the narrow rectangular troughs (Schultz 1998). This hypothesis is in agreement with the crustal thinning

observed under VM by Zuber *et al.* (2000) and with the existence of fault-like features visible in images of the valley walls (e.g., Wilkins and Schultz, 2000). The tectonic grabens were probably superimposed on a series of older basins, produced by crustal collapse, resulting in the large width of the central section of VM (Melas Chasma) (Schultz 1998). Erosional processes, i.e., the action of liquid water, were also important in producing the current geomorphology (Lucchitta *et al.* 1992; Smith *et al.* 1999b, and see Schultz 1998) and in widening the VM canyons.

Note that, even if the valley edges at VM are not themselves faults, it is likely that there will be pervasive fracturing throughout the crust; the presence of several sets of cross-cutting graben has been noted by Peulvast and Masson (1993), for example. Therefore, the calculated values of σ_{\max} will still give some estimate of the strength of faults, since if the small fractures were not able to support the imposed stresses of order σ_{\max} , movement would occur across them, decreasing the amplitude of the topography.

The elastic thickness at VM has been estimated by McKenzie *et al.* (2001), using an extension of the method of McKenzie and Nimmo (1997), but taking account of the finite amplitude of the topography (see, e.g., Parker 1972). In this method, the admittance (Lewis and Dorman 1970, McKenzie and Bowin 1976) is calculated using the line-of-sight accelerations of the Mars Global Surveyor (MGS) in its orbit, as a proxy for the gravity field, and the MOLA topography. The admittance spectrum for VM could be modeled by a best-fit elastic thickness of around 50 km, the short-wavelength admittance estimates being consistent with a crustal density of around 2.4 Mg m^{-3} . This low density may be due to an $\sim 40\%$ proportion of water ice mixed in with the bedrock. The T_e estimate may also be compared to the upper limit of 30 km calculated by Anderson and Grimm (1998) on the basis of the amplitude of the gravity anomaly which is associated with VM. Zuber *et al.* (2000) estimated T_e for the VM region, using a spatospectral localization method similar to that of Simons *et al.* (1997), which gave a value of around 60 km. In addition, McGovern *et al.* (2001) obtained elastic thickness estimates using an extension of the method of Simons *et al.* (1997). This technique yielded a T_e estimate of 50–200 km for VM.

3.2. Strength of Faults at Valles Marineris

For VM, the apparent canyon widths (“ λ ”) can be seen to vary between approximately 100 and 400 km (see Fig. 4), although the tectonically controlled sections (i.e., neglecting the erosional basins which predate the faulting; see Section 3.1) may be no wider than around 150 km (Schultz 1998, Schultz and Lin 2001). Assuming the elastic thickness at the time of formation was 50 km (see Section 3.1), upper and lower limits can be placed on σ_{\max} as follows; for $\lambda = 100$ km, $\lambda/T_e = 2$, and so $\sigma_{\max} = 12$ MPa (Eq. (2b)), while for $\lambda = 400$ km, $\lambda/T_e = 8$, and so $\sigma_{\max} = 120$ MPa (Eq. (2c)) (see Fig. 3b). Since there is again some evidence that wider canyons tend to be shallower (e.g., profile h), and because T_e is unlikely to have been less than 50 km at the time of formation, these stress values

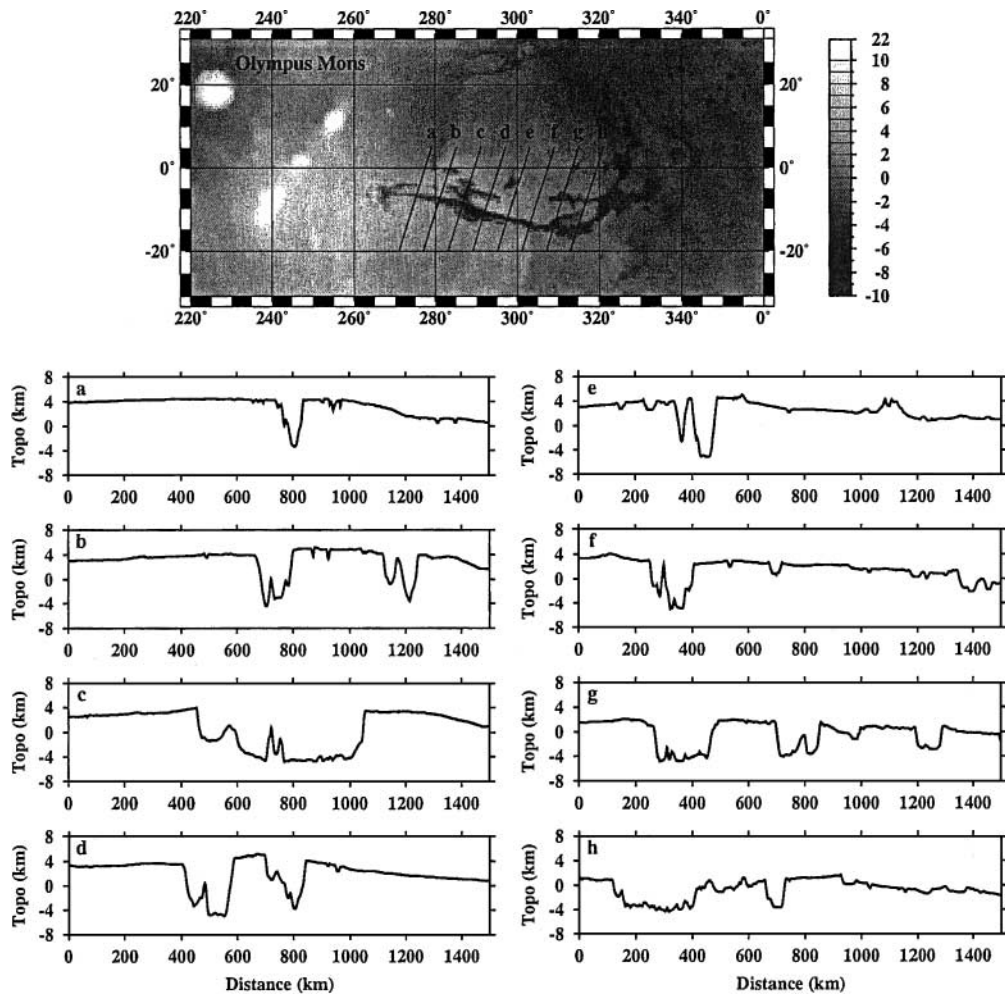


FIG. 4. Topographic profiles across Valles Marineris, as in Fig. 1. The vertical exaggeration is about $\times 22$.

are upper limits. Thus, whether or not the faults at VM are stronger than terrestrial faults depends on the width of the fault-controlled sections of the grabens. This issue is discussed further in Section 4.

4. DISCUSSION

We have assumed that the rift morphology is controlled by the maximum stresses which the bounding faults can withstand. These stresses increase with decreasing T_e and with increasing λ (see Fig. 3). For elastic thicknesses at the time of rift formation of around 20 and 50 km (or greater) at the NTR and VM, respectively, there is no evidence that the faults supporting the topography at both locations need to be able to withstand stresses greater than ~ 20 MPa, provided the tectonic widths of the grabens do not exceed 100 and 150 km, respectively. The martian topography would then not therefore require the bounding faults to be stronger than terrestrial faults. This condition is likely to be satisfied at the NTR, which of the two regions studied is the feature that more closely resembles a terrestrial

rift (Hauber and Kronberg 2001). On Earth, faults are weakened by the presence of water. Malin and Edgett (2000) have argued, on the basis of the presence of geomorphic features resembling those produced by groundwater seepage and surface runoff, that water exists in the shallow subsurface of Mars at the present day. Earlier in Mars's history, liquid water was presumably more abundant. Thus, martian faults may also have been weakened due to the presence of water.

The situation at VM is much less clear. On Mars, the value of T_e at VM at the time of its formation was probably at least 50 km (Zuber *et al.* 2000, McGovern *et al.* 2001, McKenzie *et al.* 2001), which, for the current morphology (maximum canyon widths of ~ 400 km), would require bounding fault stresses of around 100 MPa (Fig. 3b). The canyons have clearly been widened by erosive processes subsequent to their formation. Schultz (1989) and Schultz and Frey (1989) suggest widening factors of up to 3; Schultz (1991) and Lucchitta *et al.* (1994) claim, on the basis of analysis of the morphology of the valley walls, that a value of ~ 30 –70% is more reasonable. However, recent modeling by Schultz and Lin (2001), who use a lack of observed rift-flank

uplift to place limits on the likely dips of the bounding faults, suggests that most of the original fault-bounded troughs were only ~ 150 -km or less wide. Such widths would produce resolved shear stresses of 20 MPa or less (Eq. (2b)). Thus, it is possible that the faults at VM are no stronger than the faults at the NTR. However, if the present-day canyon widths are representative of the original fault-bounded trough dimensions, the VM faults must have been stronger than those at the NTR. One explanation is that the faulting at VM is more recent, probably having occurred largely in the Amazonian (Schultz 1998), whereas faulting at the NTR occurred during the Noachian and Hesperian (Golombek *et al.* 1996). Since Mars has been cooling with time, it is possible that the presence of subsurface water early in Mars' history produced weak faults; later tectonic activity may have taken place in the absence of liquid water and thus involved stronger faults.

An alternative to requiring stronger faults than on Earth would be if VM were not fault-bounded and the lithosphere were not pervasively fractured at this time; the stress required to fault intact rock is much higher than that required to move existing faults (see, e.g., Scholz 1990). Such a suggestion would have major implications for genetic models of VM, which invoke a dominantly fault-controlled origin. Note that the value of ~ 100 MPa is similar to the stresses which have been calculated to be necessary to support large loads (such as Hawaii) on the Earth (McNutt 1980), on the basis of amplitude of the gravity anomalies which are associated with such loads.

In summary, therefore, faults supporting the topography at the NTR do not need to be able to support stresses greater than those on terrestrial faults, and the same may also be true of VM. In these cases, faults are presumably weakened by pore fluid pressure and thus require the presence of liquid water within the crust over the depth range for which faulting occurs. On the basis of models of the observed fault morphology at VM, Schultz and Lin (2001) suggest that faulting continues to a depth of around 70 km. On the Earth, the depth to the base of the seismogenic layer is controlled by an isotherm of about 500–700 K (Chen and Molnar 1983). If the same is true on Mars, then, assuming a linear thermal gradient and constant conductivity, the melting temperature of water would be reached at a depth of around 9–15 km, so that most of the fault surface would indeed be in contact with liquid water, rather than with ice. In addition, such a geotherm would imply a reasonable surface heat flux of 13–22 mW m⁻².

On Venus, the lack of water results in faults which are capable of withstanding stresses around eight times greater than can be maintained on terrestrial faults. The frictional resistance to motion across venusian faults is therefore very high, which is probably the main factor controlling the lack of plate tectonics on Venus. Conversely, faults on Mars may be no stronger than those on the Earth, a fact which is probably due to the presence of water in the relatively shallow martian subsurface. However, the smaller size of Mars, compared to the Earth, means that Mars might be expected to have cooled more quickly and has a thicker lithosphere at the present day; stratigraphic cross-cutting

relationships and crater counting suggest that the Tharsis volcanoes are among the youngest features on the planet (e.g., Barlow 1988) and may have been active within the past 100 Ma (Hartmann 1977, Hartmann *et al.* 1999). Therefore, T_e estimates for these features are likely to be most representative of the strength of the lithosphere at the present day. The elastic thickness supporting the largest Tharsis volcanoes has been estimated by several authors (e.g., Thurber and Toksöz 1978, Willemann and Turcotte 1982, Comer *et al.* 1985, Janle and Janssen 1986, Zuber *et al.* 2000, McGovern *et al.* 2001) and is generally thought to be ~ 100 km or greater, in agreement with the thick lithosphere hypothesis. The stresses required to bend such a thick plate and initiate subduction, a process which is probably essential for plate tectonics to be maintained (McKenzie 1977, Conrad and Hager 1999), are therefore likely to be sufficiently large so that the driving forces for plate tectonics cannot overcome them. In addition, the thick basaltic crust may result in a positively buoyant lithosphere, which would also inhibit subduction (Zuber *et al.* 2000, Nimmo and Stevenson 2001). Thus, even if (as seems likely) faults on Mars are as weak as terrestrial faults, the other factors described are likely to contribute to the observed lack of martian plate tectonics. The existence of plate tectonics on the Earth at the present day is therefore probably due to a combination of the Earth being large enough not to have lost its heat too quickly and the weakening of faults by the presence of water in the interior, which is maintained by the subduction of hydrated oceanic crust.

ACKNOWLEDGMENTS

We thank Dan McKenzie, James Jackson, and Jeff Parke for their assistance and Richard Schultz and Patrick McGovern for their reviews. This work was carried out with the support of Schlumberger Cambridge Research, the Newton Trust, the Royal Society, Magdalene College, the California Institute of Technology, partial support by the NASA Mars Data Analysis Program, and grants from the Natural Environment Research Council and the Cambridge University Hardship Fund. This is Department of Earth Sciences, Cambridge University, Contribution Number 6801.

REFERENCES

- Anderson, S., and R. E. Grimm 1998. Rift processes at the Valles Marineris, Mars: Constraints from gravity on necking and rate-dependent strength evolution. *J. Geophys. Res.* **103**, 11,113–11,124.
- Banerdt, W. B., R. J. Phillips, N. H. Sleep, and R. S. Saunders 1982. Thick-shell tectonics on one-plate planets: Applications to Mars. *J. Geophys. Res.* **87**, 9723–9733.
- Banerdt, W. B., M. P. Golombek, and K. L. Tanaka 1992. Stress and tectonics on Mars. In *Mars* (H. H. Kieffer, B. M. Jakosky, C. W. Snyder, and M. S. Matthews, Eds.), pp. 249–297. Univ. of Arizona Press, Tucson.
- Barlow, N. G. 1988. Crater size-frequency distributions and a revised martian relative chronology. *Icarus* **75**, 285–305.
- Barton, N. 1976. The shear strength of rock and rock joints. *Int. J. Rock Mech. Mining Sci.* **13**, 255–279.

- Blasius K. R., J. A. Cutts, J. E. Guest, and H. Masursky 1977. Geology of the Valles Marineris: First analysis of imaging from the Viking 1 Orbiter primary mission. *J. Geophys. Res.* **82**, 4067–4091.
- Brace, W. F., and D. L. Kohlstedt 1980. Limits on lithostatic stress imposed by laboratory experiments. *J. Geophys. Res.* **85**, 6248–6252.
- Brown, C. D., and R. J. Phillips 1999. Flexural rift flank uplift at the Rio Grande rift, New Mexico. *Tectonics* **18**, 1275–1291.
- Byerlee, J. D. 1968. Brittle–ductile transition in rocks. *J. Geophys. Res.* **73**, 4741–4750.
- Byerlee, J. D. 1978. Friction of rocks. *Pure Appl. Geophys.* **116**, 615–626.
- Chen, W.-P., and P. Molnar 1983. Focal depths of intracontinental and intraplate earthquakes and their implications for the thermal and mechanical properties of the lithosphere. *J. Geophys. Res.* **88**, 4183–4214.
- Comer, R. P., S. C. Solomon, and J. W. Head 1985. Mars: Thickness of the lithosphere from the tectonic response to volcanic loads. *Rev. Geophys.* **23**, 61–92.
- Conrad, C. P., and B. H. Hager 1999. Effects of plate bending and fault strength at subduction zones on plate dynamics. *J. Geophys. Res.* **104**, 17,551–17,571.
- Forsyth, D. W. 1985. Subsurface loading and estimates of the flexural rigidity of continental lithosphere. *J. Geophys. Res.* **90**, 12623–12632.
- Foster, A., and F. Nimmo 1996. Comparisons between the rift systems of East Africa, Earth and Beta Regio, Venus. *Earth Planet. Sci. Lett.* **143**, 183–195.
- Frey, H. V. 1979. Martian canyons and African rifts: Structural comparisons and implications. *Icarus* **37**, 142–155.
- Golombek, M. P., and N. T. Bridges 2000. Erosion rates on Mars and implications for climate change: Constraints from the Pathfinder landing site. *J. Geophys. Res.* **105**, 1841–1853.
- Golombek, M. P., K. L. Tanaka, and B. J. Franklin 1996. Extension across Tempe Terra, Mars, from measurements of fault scarp widths and deformed craters. *J. Geophys. Res.* **101**, 26,119–26,130.
- Hartmann, W. K. 1977. Relative crater production rates on planets. *Icarus* **31**, 260–276.
- Hartmann, W. K., M. Malin, A. McEwen, M. Carr, L. Soderblom, P. Thomas, E. Danielson, P. James, and J. Veverka 1999. Evidence for recent volcanism on Mars from crater counts. *Nature* **397**, 586–589.
- Hauber, E., and P. Kronberg 2001. Tempe Fossae, Mars: A planetary analog to a terrestrial continental rift? *J. Geophys. Res.* **106**, 20,587–20,602.
- Jackson, J. A., and N. J. White 1989. Normal faulting in the upper continental crust: Observations from regions of active extension. *J. Struct. Geol.* **11**, 15–36.
- Janle P., and D. Janssen 1986. Isostatic gravity and elastic bending models of Olympus Mons, Mars. *Ann. Geophys.* **4**, 537–546.
- Lachenbruch, A. H., and J. H. Suss 1988. The stress heat-flow paradox and thermal results from Cajon Pass. *Geophys. Res. Lett.* **15**, 981–984.
- Le Pichon, X., J. Francheteau, and J. Bonnin 1976. *Developments in Geotectonics: Plate Tectonics*, Vol. 6. Elsevier Press, New York.
- Lewis, B. T. R., and L. M. Dorman 1970. Experimental Isostasy. 2. An isostatic model for the U.S.A. derived from gravity and topographic data. *J. Geophys. Res.* **75**, 3367–3386.
- Lucchitta, B. K., A. S. McEwen, G. D. Clow, P. E. Geissler, R. B. Singer, R. A. Schultz, and S. W. Squyres 1992. The canyon system on Mars. In *Mars* (H. H. Kieffer, B. M. Jakosky, C. W. Snyder, and M. S. Matthews, Eds.), pp. 453–492. Univ. of Arizona Press, Tucson.
- Lucchitta, B. K., N. K. Isbell, and A. Howington-Kraus 1994. Topography of Valles Marineris: Implications for erosional and structural history. *J. Geophys. Res.* **99**, 3783–3798.
- Lyon-Caen, H., and P. Molnar 1983. Constraints on the structure of the Himalaya from an analysis of gravity anomalies and a flexural model of the lithosphere. *J. Geophys. Res.* **88**, 8171–8191.
- Maggi, A., J. A. Jackson, D. McKenzie, and K. Priestley 2000. Earthquake focal depths, effective elastic thickness, and the strength of the continental lithosphere. *Geology* **28**, 495–498.
- Malin, M. C., and K. S. Edgett 2000. Evidence for recent groundwater seepage and surface runoff on Mars. *Science* **288**, 2330–2335.
- McGovern, P. J., S. C. Solomon, D. E. Smith, M. T. Zuber, G. A. Neumann, J. W. Head, R. J. Phillips, and M. Simons 2001. Gravity/topography admittances and lithospheric evolution on Mars: The importance of finite-amplitude topography. *Lunar Planet. Sci.* **32**, Abstract 1804.
- McKenzie, D. 1967. Some remarks on heat flow and gravity anomalies. *J. Geophys. Res.* **72**, 6261–6263.
- McKenzie, D. 1977. The initiation of trenches: A finite amplitude instability. In *Island Arcs, Deep Sea Trenches and Back-Arc Basins* (M. Talwani and W. C. Pitman III, Eds.), pp. 57–62. Maurice Ewing Series 1, Am. Geophys. Union, Washington, DC.
- McKenzie, D., and C. Bowin 1976. The relationship between bathymetry and gravity in the Atlantic Ocean. *J. Geophys. Res.* **81**, 1903–1915.
- McKenzie, D., and D. Fairhead 1997. Estimates of the effective elastic thickness of the continental lithosphere from Bouguer and free air gravity anomalies. *J. Geophys. Res.* **102**, 27,523–27,552.
- McKenzie, D., and F. Nimmo 1997. Elastic thickness estimates for Venus from line of sight accelerations. *Icarus* **130**, 198–216.
- McKenzie, D., D. N. Barnett, and D.-N. Yuan 2001. The relationship between martian gravity and topography. *Earth Planet. Sci. Lett.* **195**, 1–16.
- McNutt, M. 1980. Implications of regional gravity for state of stress in the Earth's crust and upper mantle. *J. Geophys. Res.* **85**, 6377–6396.
- Mount, V. S., and J. Suppe 1987. State of stress near the San Andreas fault: Implications for wrench tectonics. *Geology* **15**, 1143–1146.
- Nimmo, F., and D. McKenzie 1998. Volcanism and tectonics on Venus. *Annu. Rev. Earth Planet. Sci.* **26**, 23–51.
- Nimmo, F., and D. J. Stevenson 2001. Estimates of martian crustal thickness from viscous relaxation of topography. *J. Geophys. Res.* **106**, 5085–5098.
- Nyquist, J. E., and H. F. Wang 1988. Flexural modeling of the Midcontinent Rift. *J. Geophys. Res.* **93**, 8852–8868.
- Parker, R. L. 1972. The rapid calculation of potential anomalies. *Geophys. J. R. Astr. Soc.* **31**, 447–455.
- Peulvast, J. P., and P. L. Masson 1993. Erosion and tectonics in central Valles Marineris (Mars): A new morpho-structural model. *Earth, Moon Planets* **61**, 191–217.
- Rice, J. R. 1992. Fault stress states, pore pressure distributions and the weakness of the San Andreas Fault. In *Fault Mechanics and Transport Properties of Rocks* (B. Evans and T.-F. Wong, Eds.), pp. 475–503. Academic Press, San Diego.
- Scholz, C. H. 1982. Scaling laws for large earthquakes: Consequences for physical models. *Bull. Seism. Soc. Am.* **72**, 1–14.
- Scholz, C. H. 1990. *The Mechanics of Earthquakes and Faulting*. Cambridge Univ. Press, Cambridge, UK.
- Scholz, C. H. 2000. Evidence for a strong San Andreas fault. *Geology* **28**, 163–166.
- Schultz, R. A. 1989. Do pit crater chains grow up to be Valles Marineris canyons? In *Proceedings of MEVTV Workshop on Tectonic Features on Mars* (T. R. Watters and M. P. Golombek, Eds.), pp. 47–48 (abstract). LPI Technical Report 89-06.
- Schultz, R. A. 1991. Structural development of Coprates Chasma and western Ophir Chasma, Valles Marineris rift, Mars. *J. Geophys. Res.* **96**, 22,777–22,792.
- Schultz, R. A. 1998. Multiple-process origin of Valles Marineris basins and troughs, Mars. *Planet. Space Sci.* **46**, 827–834.
- Schultz, R. A., and H. V. Frey 1989. Topography and structure of Valles Marineris, Mars, presented at Fourth International Conference on Mars, Tucson, Arizona, Jan. 10–13.

- Schultz, R. A., and J. Lin 2001. Three-dimensional normal faulting models of the Valles Marineris, Mars, and geodynamic implications. *J. Geophys. Res.* **106**, 16,549–16,566.
- Sharp, R. P. 1973. Mars: Troughed terrain. *J. Geophys. Res.* **78**, 4063–4072.
- Simons, M., S. C. Solomon, and B. H. Hager 1997. Localization of gravity and topography: Constraints on the tectonics and mantle dynamics of Venus. *Geophys. J. Int.* **131**, 24–44.
- Sleep, N. H., and M. L. Blampied 1992. Creep, compaction and the weak rheology of major faults. *Nature* **359**, 687–692.
- Smith, D., G. Neumann, P. Ford, R. E. Arvidson, E. A. Guinness, and S. Slavney 1999a. Mars Global Surveyor Laser Altimeter Initial Experiment Gridded Data Record, NASA Planetary Data System, MGS-M-MOLA-5-IEGDR-L3-V2.0. PDS label for Mars topographic grid MOLA-IEG0062T, available at http://wufs.wustl.edu/mgs/mgsl_2033/data/egdr/ieg0062t.lbl.
- Smith, D. E., M. T. Zuber, S. C. Solomon, R. J. Phillips, J. W. Head, J. B. Garvin, W. B. Banerdt, D. O. Muhleman, G. H. Pettengill, G. A. Neumann, F. G. Lemoine, J. B. Abshire, O. Aharonson, C. D. Brown, S. A. Hauck, A. B. Ivanov, P. J. McGovern, H. J. Zwally, and T. C. Duxbury 1999b. The global topography of Mars and implications for surface evolution. *Science* **284**, 1495–1502.
- Tanaka, K. L., and M. P. Golombek 1989. Martian tension fractures and the formation of grabens and collapse features at Valles Marineris. *Proc. Lunar Planet. Sci. Conf.* **19**, 383–396.
- Tanaka, K. L., D. H. Scott, and R. Greeley 1992. Global stratigraphy. In *Mars* (H. H. Kieffer, B. M. Jakosky, C. W. Snyder, and M. S. Matthews, Eds.), pp. 345–382. Univ. of Arizona Press, Tucson.
- Thurber, C. H., and M. N. Toksöz 1978. Martian lithospheric thickness from elastic flexure theory. *Geophys. Res. Lett.* **5**, 977–980.
- Watts, A. B. 1994. Crustal structure, gravity anomalies and flexure of the lithosphere in the vicinity of the Canary Islands. *Geophys. J. Int.* **119**, 648–666.
- Willemann, R. J., and D. L. Turcotte 1982. The role of lithospheric stress in the support of the Tharsis Rise. *J. Geophys. Res.* **87**, 9793–9801.
- Wilkins, S. J., and R. A. Schultz 2000. Cross faults in extensional settings: Stress triggering, displacement localization and implications for the origin of blunt-troughs in Valles Marineris, Mars. *J. Geophys. Res.*, submitted.
- Wilkins, S. J., and R. A. Schultz 2001. Structural style and mode of extension in the northern Tempe rift. *Lunar Planet. Sci.* **32**, Abstract 1253.
- Wright, T., E. Fielding, and B. Parsons 2001. Triggered slip: Observations of the 17 August 1999 Izmit (Turkey) earthquake using radar interferometry. *Geophys. Res. Lett.* **28**, 1079–1082.
- Yuan, D.-N., W. L. Sjogren, A. S. Konopliv, and A. B. Kucinskis 2001. The gravity field of Mars: A 75th degree and order model. *J. Geophys. Res.* **106**, 23377–23401.
- Zoback, M. D., and G. C. Beroza 1993. Evidence for near-frictionless faulting in the 1989 (M 6.9) Loma Prieta, California, earthquake and its aftershocks. *Geology* **21**, 181–185.
- Zuber, M. T., S. C. Solomon, R. J. Phillips, D. E. Smith, G. L. Tyler, O. Aharonson, G. Balmino, W. B. Banerdt, J. W. Head, C. L. Johnson, F. G. Lemoine, P. J. McGovern, G. A. Neumann, D. D. Rowlands, and S. Zhong 2000. Internal structure and early thermal evolution of Mars from Mars Global Surveyor topography and gravity. *Science* **287**, 1788–1793.